Atmos. Chem. Phys. Discuss., https://doi.org/10.5194/acp-2019-466
Manuscript under review for journal Atmos. Chem. Phys.
Discussion started: 21 May 2019

Atmospheric Chemistry and Physics Discussions

CCN concentration and INP-relevant aerosol profiles in the Saharan Air Layer over Barbados from polarization lidar and airborne in situ measurements

Moritz Haarig[1], Adrian Walser[2], Albert Ansmann[1], Maximilian Dollner[2], Dietrich Althausen[1], Daniel Sauer[3], David Farrell[4], and Bernadett Weinzierl[2]

[1]Leibniz Institute for Tropospheric Research (TROPOS), Leipzig, Germany
[2]Faculty of Physics, University of Vienna, Vienna, Austria
[3]Deutsches Zentrum für Luft- und Raumfahrt (DLR), Oberpfaffenhofen, Germany
[4]Caribbean Institute for Meteorology and Hydrology, Bridgetown, Barbados

Correspondence to: Moritz Haarig (haarig@tropos.de)

Abstract. The present study aims to validate lidar retrievals of cloud-relevant aerosol properties by using polarization lidar and coincident airborne in situ measurements in the Saharan Air Layer over the Barbados region. Vertical profiles of the number concentration of cloud condensation nuclei (CCN), large particles (diameter d>500 nm), surface area, and ice nucleating particles (INP) are estimated from the lidar measurements and compared with CCN concentrations and the INP-relevant aerosol properties in situ measured with aircraft in the framework of the Saharan Aerosol Long-range Transport and Aerosol–Cloud-interaction Experiment (SALTRACE) in summer 2013. The CCN number concentrations derived from lidar observations were up to a factor of two higher than the ones measured in situ on board the research aircraft Falcon. However, a reasonable agreement was obtained when taking the lidar uncertainty into account. The number concentration of particles with dry radius >250 nm and the surface area concentration obtained from the lidar observations and used as input for the INP parameterizations agreed well (<30–50% deviation) with the aircraft measurements. In a pronounced lofted dust layer during summer (10 July 2013), the lidar retrieval yielded 100–300 CCN per cm^3 at 0.2% water supersaturation and 25–65 INP per L at –25°C. During the SALTRACE winter campaign (March 2014), the dust layer from Africa was mixed with smoke particles which dominated the CCN number concentration. This example highlights the unique lidar potential to separate smoke and dust contributions to the CCN reservoir and thus to identify the sensitive role of smoke in trade wind cumuli developments over the tropical Atlantic during the winter season.

1 Introduction

Climate predictions are highly uncertain (IPCC, 2013). One of the reasons is our poor knowledge of the impact of atmospheric aerosols on cloud processes. To improve our understanding of aerosol-cloud interaction, new techniques for profiling of cloud condensation nuclei (CCN) and ice-nucleating particles (INP) are required. Lidar permits a regular and continuous monitoring of the cloud-relevant aerosol properties up to the tropopause height. Methods have been developed to retrieve CCN and INP-relevant particle microphysical properties from particle extinction coefficients measured with lidar (Mamouri and Ansmann,

2016; Lv et al., 2018). In the case of INP profiling, particle extinction coefficients are converted to particle number concentrations n_{250} (particles with dry radius >250 nm) and particle surface area concentrations s. The n_{250} profile is input in the INP parameterization schemes of DeMott et al. (2010, 2015, 2016) and Tobo et al. (2013) and s profiles are input in respective INP parameterizations by Niemand et al. (2012), Steinke et al. (2015), Ullrich et al. (2017), and McCluskey et al. (2018). The entire lidar-based INP lidar retrieval procedure is described by Mamouri and Ansmann (2016). First comparisons of the CCN lidar retrievals with airborne in situ observations over a polluted Central European site are presented by Düsing et al. (2018). First comparisons regarding INP can be found in Schrod et al. (2017) and Marinou et al. (2018). These observations were conducted in the dusty and polluted Eastern Mediterranean (Cyprus).

In this article, we present for the first time comparison of airborne in situ and ground-based lidar observations of CCN number concentration and INP-relevant aerosol properties for aged dust over the remote Atlantic several 1000 km west of the source regions in Africa. We use the opportunity of the SALTRACE campaign (Saharan Aerosol Long-range Transport and Aerosol–Cloud-interaction Experiment, Weinzierl et al., 2017), conducted in the Caribbean (Barbados region), for this goal. More than 12 weeks of lidar measurements were performed in June–July 2013 (SALTRACE-1), February–March 2014 (SALTRACE-2), and June–July 2014 (SALTRACE-3). A triple-wavelength polarization Raman lidar (Haarig et al., 2017a) of the Leibniz Institute for Tropospheric Research (TROPOS) was operated at the Caribbean Institute for Meteorology and Hydrology (CIMH), north of Bridgetown, Barbados (13.15°N, 59.62°W, 110 m about sea level). Airborne in situ measurements were performed during SALTRACE-1. An overview of the instrumentation on-board the research aircraft Falcon of the German Aerospace Center (Deutsches Zentrum für Luft- und Raumfahrt – DLR) is given by Weinzierl et al. (2017).

SALTRACE observations of the long-range transported Saharan dust have been published in the SALTRACE special issue (Groß et al., 2015; Haarig et al., 2017a; Gasteiger et al., 2017; Kandler et al., 2018). The lofted dust plumes in the Saharan air layer (SAL) occur between 1.5–5 km height. Many simultaneous measurements with aircraft and the ground based lidar have been realized during SALTRACE. For our study, we use the Falcon observations of the particle size distribution and of the CCN number concentration. In the lidar-Falcon comparisons, three case studies are analyzed. CCN properties have been studied previously in the Caribbean but without involving vertical profiling with lidar (Siebert et al., 2013; Kristensen et al., 2016; Wex et al., 2016; Jung et al., 2016). A dust–smoke mixture from the SALTRACE-2 (winter campaign) is presented in addition to contrast the almost pure dust conditions prevailing during the summer half year with the aerosol conditions during the winter half year when the Saharan dust plumes are mixed with biomass burning smoke. This comparison highlights the strong impact of smoke particles on the CCN levels over the remote tropical Atlantic during the winter half year (biomass burning season).

The paper is structured as follows: In Sect. 2, the ground-based and airborne instrumentation and the lidar retrieval are shortly presented. Then the three Saharan dust cases (used in our comparison study) are described regarding dust layering, the meteorological context, and air mass transport (Sect. 3). In Sect. 4, CCN concentrations and particle number, surface area and mass concentrations obtained from the aircraft and lidar measurements are compared. In Sect. 5, summer and winter SAL lidar observations are contrasted. A summary and concluding remarks are given in the last section.

Atmos. Chem. Phys. Discuss., https://doi.org/10.5194/acp-2019-466
Manuscript under review for journal Atmos. Chem. Phys.
Discussion started: 21 May 2019

Atmospheric Chemistry and Physics Discussions

2 Instrumentation and methods

2.1 Lidar retrievals of CCN and INP concentrations

The triple-wavelength polarization Raman lidar BERTHA (Backscatter, Extinction, lidar Ratio, Temperature, Humidity profiling Apparatus) described in Haarig et al. (2017a) measures the backscatter coefficient at three wavelengths (355, 532, and 1064 nm), the extinction coefficient at 355 and 532 nm and in a new configuration also at 1064 nm (Haarig et al., 2016). The depolarization ratio is measured at 355, 532, and 1064 nm simultaneously. During the SALTRACE campaigns in 2013–2014, the lidar was deployed at the Caribbean Institute for Meteorology and Hydrology (CIMH), at Husbands, 5 km north of the capital Bridgetown, Barbados.

The conversion from backscatter coefficient and particle linear depolarization ratio (PLDR) to particle number and surface area concentration follows the method described in Mamouri and Ansmann (2016). The particle depolarization ratio is used to separate the contributions of different aerosol types (mineral dust (d), marine aerosol (m), and continental aerosol (c)) to the backscatter coefficient. By multiplication with an appropriate extinction-to-backscatter ratio (lidar ratio, S_d=55 sr, S_m=20 sr, S_c=50 sr) the backscatter coefficients are converted into extinction coefficients. Empirical conversion factors (Mamouri and Ansmann, 2016; Ansmann et al., 2019) are applied to derive particle number concentrations from the extinction coefficients. The respective equations and the conversion factors are listed in Table 1. The conversion factors are based on long-term AERONET observations (particle size distributions and AOD, Holben et al., 1998), filtered for dust events (Ångström exponent AE<0.3, AOT>0.1 at 500 nm), pure marine (0.25<AE<0.6, AOT<0.07) and continental (AE>1.6) conditions (Mamouri and Ansmann, 2016; Ansmann et al., 2019) . It should be mentioned that the conversion factor for small continental aerosol particles ($n_{50,c}$, particles with diameter >100 nm), is obtained using AERONET data from Leipzig (Central Europe), but with a factor of 0.5 to best approximate the African rural aerosol conditions (Shinozuka et al., 2015).

In a next step, INP and CCN concentrations are retrieved. INP parameterizations have been developed for the aerosol types dust, soot, and marine particles (see Table 2). The number concentration n_{250} and the surface area concentration s are the aerosol-relevant input parameters and are again obtained by conversion of the lidar-derived particle extinction profiles into the respective microphysical properties. In the present study, we focus on immersion freezing, i.e., ice nucleation by an INP immersed into a liquid-water droplet. The INP parameterizations and input parameters are listed in Table 2. In this study, we focus on the n_{250}-based parameterizations.

To estimate the CCN number concentration n_{CCN}, Mamouri and Ansmann (2016) use a dry activation diameter of 200 nm for dust and 100 nm for continental pollution and marine particles at 0.15–0.2% water supersaturation. A factor f_{ss} is used to retrieve n_{CCN} for different supersaturation levels (see Table 1).

The use of the different activation diameters (100 nm for continental pollution aerosol and for marine particles, 200 nm for dust) is motivated by the following facts. Based on kappa-Köhler theory (Petters and Kreidenweis, 2007), we computed the critical activation diameter for 0.2% water supersaturation and temperatures from –10°to 20°C for various materials and chemical compositions (see Table 3), in which 10°C is the most realistic value within the SAL as indicated by local radiosondes. Fresh Saharan dust is very hydrophobic (low hygroscopicity parameter κ) so that the activation diameter is around 275 nm (at

10°C). Cloud-processed Saharan dust particles may have changed their hygroscopic properties (higher κ value) so that their CCN efficacy increased. Laboratory studies with wet-generated dust particles (in contrast to dry-generated fresh dust particles) reported higher κ values (Koehler et al., 2009; Herich et al., 2009; Kumar et al., 2011b). However, although the Saharan dust was transported over several thousands of kilometers across the Atlantic Ocean, observations suggest that the dust in the SAL remained nearly unprocessed (Lieke et al., 2011; Denjean et al., 2015; Weinzierl et al., 2017; Kandler et al., 2018) so that κ should be closer to the value for fresh Saharan dust. Herich et al. (2009) concluded that the activation diameter for Saharan dust (dry generated) is most probably 200 nm at a supersaturation of 0.2%. This is confirmed by studies of Shinozuka et al. (2015) and Lv et al. (2018).

The activation diameter for continental aerosol particles (fine-mode pollution) depends on their chemical composition. Kandler et al. (2018) found sulfate particles as a dominant contribution of continental pollution aerosol in the SAL, but the instrumentation was not suitable to detect organics. Considering ammonium sulfate with a small contribution of less hydrophilic organic particles as continental aerosol within the SAL, a dry activation diameter of 100 nm at a supersaturation of 0.2% is a suitable estimate and therefore used in this study.

The very hydrophilic sea salt particles (sodium chloride) have an activation diameter of 70 nm (see Table 3, at 0.2% supersaturation and 10°C). Whereas Mamouri and Ansmann (2016) estimated a dry activation diameter of 100 nm based on literature. Going from 100 nm to 70 nm as activation diameter, would increase n_{CCN} by a factor of approximately 1.5. In conclusion, we used a dry activation diameter of 200 nm for Saharan dust, and of 100 nm for continental and marine particles, assuming a supersaturation of 0.2%, in the SALTRACE studies.

The polarization lidar–photometer networking technique (POLIPHON) introduced by Mamouri and Ansmann (2014, 2017) delivers mass concentrations of fine and coarse mode dust, i.e, dust particles with diameter d<1 μm and d>1 μm, respectively (see Table 1). The PLDR at 532 nm is used to separate the contributions of non-dust aerosol (PLDR=0.05), fine mode dust (PLDR=0.16), and coarse mode dust (PLDR=0.35).

2.2 Airborne in situ aerosol measurements

A full list and details of the instrumentation installed aboard the research aircraft Falcon of the DLR are given in Weinzierl et al. (2017). Information on size-resolved particle number concentrations are obtained from condensation particle counters and optical particle spectrometers. The condensation particle counters were operated at slightly different cutoff diameters around 10 nm. The spectrometer setup included an airborne version of the Ultra High Sensitivity Aerosol Spectrometer (Cai et al., 2008; Brock et al., 2011; Kupc et al., 2018), a Grimm model 1.129 SkyOPC, and a Cloud and Aerosol Spectrometer (Baumgardner et al., 2001). The combination of these spectrometers covers the complete range of particle diameters from about 70 nm to 50 μm. Particle number size distributions (NSDs) are derived from the entirety of these data using a consistent Bayesian inversion method (Walser et al., 2017). Here, the NSDs are approximated by trimodal log-normal distributions. In situ cloud condensation nuclei concentrations are measured with a Cloud Condensation Nuclei Counter (Roberts and Nenes, 2005; Lance et al., 2006) operated at a water vapor supersaturation of 0.2%. These concentrations are corrected for losses of large CCN at the aircraft's isokinetic aerosol inlet (Spanu et al., 2019).

Atmos. Chem. Phys. Discuss., https://doi.org/10.5194/acp-2019-466
Manuscript under review for journal Atmos. Chem. Phys.
Discussion started: 21 May 2019

3 Lidar observations of SAL dust layering: Comparison days

Three cases of the SALTRACE summer-2013 campaign were selected for in-depth comparisons of lidar and aircraft observations: 22 June, 10 July, and 11 July 2013. The criteria for the selection were based on the low spatial distance between the lidar site and the Falcon aircraft (flight patterns in the Barbados region, see Fig. 1). The time-height displays of the range-corrected signal at 532 nm (cross-polarized component) shown in Fig. 2 indicate very homogeneous dust structures in the SAL on these three days and thus good conditions for comparisons. Table 4 contains information about the measurement periods of the Falcon aircraft and the lidar including the mean horizontal distance of the Falcon from the lidar site and flight height levels. Except for two flight legs, the mean distance was below 100 km. In the SAL, winds from eastward directions with a wind speed between 10 and 18 m/s prevailed leading to a dust transport of 35–65 km/h. The lidar profiles were averaged over 100–140 minutes which corresponds to a spacial average of 60–150 km considering the wind speed. Therefore, the Falcon aircraft and the ground-based lidar observed in principle the same dust layer at these selected days.

A weak dust outbreak was observed on 22 June 2013 (Fig. 2a–b), belonging to the first out of four main dust periods during SALTRACE-1 (Groß et al., 2015). The trajectories (not shown) indicate a possible dust uptake over Mali and Mauritania 8–9 days prior to the arrival at Barbados. In contrast to the later two cases, these air masses spent more time in the populated coastal region of west Africa (Senegal) and so the probability of anthropogenic influence was high.

After the passage of the tropical storm Chantal (Weinzierl et al., 2017), a strong and stable flow of Saharan dust towards the Caribbean established and lasted for more than 4 days (10–13 July 2013). We use the 10 and 11 July observations for the comparison study. The Saharan Air Layer (SAL) extended vertically from 1.8 km to almost 5 km height as shown in Fig. 2c-f. As already discussed in Haarig et al. (2017a) based on backward trajectory analysis and the particle depolarization ratio measurements, pure dust conditions (with rather low probability of contamination with anthropogenic pollution) were given. The dust traveled 5–7 days over the Atlantic Ocean.

Daytime lidar observations are used to have coincident measurements with the Falcon aircraft. Below 2 km height, trade wind cumuli disturbed the lidar measurements. Only the cloud-free profiles were used for the calculation of the backscatter coefficient and depolarization ratio. These quantities (at 532 nm) are shown for the three selected cases in Fig. 2. Pure Saharan dust has a PLDR at 532 nm of 0.31±0.03 (Freudenthaler et al., 2009). The depolarization ratio (Fig. 2) indicates that not only dust was transported in the SAL. On 10 and 11 July 2013, however, only a rather small non-dust component was present (layer mean PLDR of 0.29±0.02 and 0.31±0.02, respectively). In contrast, on 22 June 2013 the non-dust component was significant (PLDR of 0.25±0.03). The indicated uncertainty considers systematic errors and statistic uncertainties in the lidar data analysis. The method described in Ansmann et al. (2017) was used to decide whether the non-dust component was of marine or continental origin. Continental aerosol has a significantly higher lidar ratio than marine aerosol (50 sr instead of 20 sr). By comparing the sum of the type-separated backscatter coefficients multiplied by respective type-dependent lidar ratios with the independently derived total particle extinction coefficient in the SAL (from our Raman lidar measurements Ansmann et al., 1992), a good agreement was found for continental pollution aerosol in the SAL. Some of the Raman lidar observation could

Atmos. Chem. Phys. Discuss., https://doi.org/10.5194/acp-2019-466
Manuscript under review for journal Atmos. Chem. Phys.
Discussion started: 21 May 2019

Atmospheric Chemistry and Physics Discussions

not be performed at bright daylight conditions. In these cases, we had to use Raman lidar measurements after sunset to check the non-dust aerosol type in the SAL as well as in the marine boundary layer.

4 Lidar versus airborne in situ aerosol observations

We begin with comparisons of CCN concentrations (n_{CCN}) in Sect. 4.1. Particle number concentrations n_{250} of large particles and surface area concentration s are then compared in Sect. 4.2. In Sect. 4.3, we show simultaneous observed profiles of fine mode and coarse mode mass concentrations.

4.1 CCN profiles

In Figure 3, the lidar-derived number concentration of CCN for dust $n_{\mathrm{CCN},d}$ (red line) and continental pollution particles $n_{\mathrm{CCN},c}$ (olive line) are presented. The total CCN number concentration n_{CCN} (black line, lidar) can be compared with measurements of the cloud condensation nuclei counter on board the Falcon aircraft (black dots) at the same supersaturation. The lidar-derived n_{CCN} values are up to twice as large as the in situ measured values. However, the lidar retrieval uncertainty (conversion factor uncertainty) is large (factor 2–3) and may be the reason for the discrepancies. In Table 5, the vertically averaged values are compared. Besides the large retrieval uncertainty, other uncertainty sources may have contributed to the systematic bias between the lidar and airborne in situ observations: (i) The lidar conversion factors are derived for AERONET stations close to the Sahara. These conversion factors may not be applicable to aged dust after long-range transport, and may overestimate the occurring accumulation mode dust particle number concentration and thus $n_{100,d}$. (ii) The used dust activation diameter (d_{dry}=200 nm) may have been too low and the true one was much larger than 200 nm (see Table 3, d=275 nm for fresh dust) and thus less dust particles were activated in the cloud condensation nuclei counter aboard the Falcon than estimated by lidar. (iii) Horizontal and temporal inhomogeneities in the dust concentration along the flight tracks and over the lidar site may have also contributed to the found differences. (iv) Although the Falcon data are corrected for the particles losses at the inlets (Spanu et al., 2019), there are several uncertainty sources in the in situ CCN retrieval, that may have contributed to the found bias.

4.2 INP-relevant aerosol profiles

In Figure 4a–c, the profiles of the sum of $n_{250,\mathrm{d}}$ and $n_{250,\mathrm{c}}$ are compared with the integral values of the particles number size distribution for d_{dry}>500 nm measured on board the Falcon aircraft. The values usually stored for standard temperature and pressure conditions are transformed to values for actual atmospheric conditions to be comparable with the lidar data. As can be seen, the in situ and lidar values agree well, except on 22 June and 11 July in the lower part of the SAL, where horizontal inhomogeneities in the dust load (see Fig. 2) may have partly caused the differences between the two measurements. The contribution of continental smoke and pollution aerosol to n_{250} was less than 3% in the SAL during the strong dust outbreak on 10–11 July 2013 and about 10% on 22 June 2013. In total, there were less than 40 particles (d_{dry}>500 nm) per cm^3 in all three cases over the remote Atlantic.

Atmos. Chem. Phys. Discuss., https://doi.org/10.5194/acp-2019-466
Manuscript under review for journal Atmos. Chem. Phys.
Discussion started: 21 May 2019

Fig. 4d–f compares the profiles of the total surface area concentration estimated from lidar extinction coefficients and derived from the airborne in situ measured number size distribution. Here, the contribution of the continental pollution particles to s within the SAL is 4–6% during the strong dust outbreak (10–11 July) and 20% on 22 June 2013. The lidar values are considerably larger than the in situ values. The use of too large conversion factors (based on AERONET observations close to the Sahara) may be one of the reasons for the strong disagreement. On the other hand, a few large particles missing in the in situ data analysis can cause a sensitive underestimation of the surface area.

An example on INP profiling is given in Fig. 4g–h. The DeMott et al. (2010, 2015) parameterization is used with $n_{250,\mathrm{d}}$ and $n_{250,\mathrm{c}}$ profiles as input. As can be seen, the SAL contains INP concentrations of 10–100 L^{-1} at –25°C. This is a comparably large INP concentration and can trigger significant heterogeneous ice formation in convective cloud systems with cloud base in the SAL when air parcels in updrafts reach the –25°C temperature level.

4.3 Fine and coarse mode mass concentrations

As an additional feature to the CCN and INP profiles, the dust mass concentration can be derived from the lidar measurements separately for fine and coarse mode dust (see Table 1). The comparison with airborne in situ observations are shown in Fig. 5. The mass concentrations are calculated from the lidar derived and in situ measured volume concentration by assuming a dust mass density of 2.6 g/cm^3. An excellent agreement is obtained for the coarse mode. This indicates that the Falcon measurements capture well the large particles in the SAL (Spanu et al., 2019). The coarse mode mass concentration from POLIPHON is around 16 times higher than the fine mode mass concentration leading to a mass fine mode fraction of 0.06. For the optical properties, such as the backscatter coefficient, the fine mode fraction is 0.2. These mass (or volume) and backscatter fractions are in full agreement with simultaneous AERONET photometer observations of the fine-mode volume and AOD fractions at Ragged Point, Barbados. Again a relatively large disagreement is found for the fine particle dominated quantities, i.e., the fine-mode mass concentration. We can only speculate about the reasons. Wrong in situ particle counting or wrong conversion factors might be the reasons. However, a good agreement of the lidar products with AERONET observations is found and corroborates the quality of the lidar products.

5 Contrasting pure dust with mixed smoke–dust conditions

During the SALTRACE-2 winter campaign (Haarig et al., 2017b), a pronounced dust outbreak reached Barbados in the beginning of March 2014. The trajectories ending at 2000 m above ground level on 3 March 2014 (not shown) point to the Sahara as dust source and West Africa (Senegal, Guinea) regarding the source region for biomass burning smoke. The transport across the Atlantic Ocean took around 2 weeks. We use the opportunity of the dust–smoke aerosol mixtures to highlight the strong impact of smoke on the CCN conditions. The transport of biomass burning smoke from Africa towards South America and the Caribbean during wintertime has been previously reported (Ansmann et al., 2009; Baars et al., 2011; Zuidema et al., 2018). An indication for the strong smoke contribution to the measured backscatter signal was the relatively low particle depolarization ratio. Fine-mode smoke does not depolarize laser light (PLDR $\leq$0.05). Figure 6 gives an overview of the measurements on

Atmos. Chem. Phys. Discuss., https://doi.org/10.5194/acp-2019-466
Manuscript under review for journal Atmos. Chem. Phys.
Discussion started: 21 May 2019

3 March 2014. A lofted layer (1.6–3.1 km height) of dust and smoke was found above the marine aerosol layer reaching to 1.6 km height. The vertical profiles in Fig. 6b and c show mean values for the time interval from 22:30 to 23:20 UTC. The particle backscatter coefficient (Fig. 6b) is separated into a dust component and a non-dust component using the PLDR separation technique (Tesche et al., 2009, 2011). To estimate whether the non-dust component is of marine or continental origin, the extinction coefficient was calculated from the different contributions to the backscatter coefficient as shown in Ansmann et al. (2017). The dust-related backscatter coefficient was multiplied by the dust lidar ratio (S_d=55 sr), and the non-dust backscatter coefficient by the lidar ratio for marine particles (S_m=20 sr, contributing to the blue curve in Fig. 6c) and for continental pollution particles (S_c=50 sr, contributing to the green curve in Fig. 6c). The sum of the extinction coefficient (dust + marine and dust + continental) is then compared with the total extinction coefficient (black curve in Fig. 6c) derived independently with the Raman lidar method (Ansmann et al., 1992). As can be seen, the lofted aerosol layer obviously contains a mixture of dust and smoke, whereas the layer below is dominated by marine particles.

In the next step, $n_{100,d}$, $n_{50,c}$, and $n_{50,m}$ (Fig. 6d) are computed, and the resulting n_{CCN} (Fig. 6e) at 0.2% supersaturation is calculated. The continental pollution contribution to the CCN number concentration is 4 times stronger than the one from the dust aerosol. Thus, in the winter half year with significant smoke contribution from Africa, rather different CCN conditions are found across the Atlantic, compared to the summer dust layers, leading to changes in the trade wind cumulus cloud developments compared to the summer months when dust particles are dominating the CCN reservoir.

In contrast, n_{250} is dominated by mineral dust (Fig. 6f). The contributions to the surface area concentration (Fig. 6g) of dust and smoke are equal. The INP concentration at –25°C estimated in Fig. 6h show a weak contribution of marine particles with 3–5 orders of magnitude less efficiency than the dust particles in the lofted layer. The immersion-freezing INP parameterizations based on n_{250} (DeMott et al., 2010, 2015) lead to values around 10 L^{-1}. The results are added in Table 5.

Fig. 7 highlights the sensitive impact of smoke aerosol on the CCN concentration. The dust contribution to the optical properties (Fig. 7a) is almost 100% in summer during strong dust outbreaks and around 50% during the biomass burning season, which is in full agreement with AERONET observations. Dust dominates the aerosol mass concentration in the SAL (Fig. 7b) throughout the year, disregarding summer or winter conditions. In strong contrast, the smoke CCN concentration (Fig. 7c) strongly varies between summer and winter. CCN levels are 200–300 cm^{-3} during strong dust outbreaks in summer (dust contribution around 80%), but close to 500 cm^{-3} observed in the March 2014 event with a strong contribution of smoke particles (80%).

6 Summary and conclusion

We compared for the first time lidar derived concentrations of CCN, particle number (n_{250}) and total surface area with airborne in situ measurements in long-range transported Saharan dust. We found good agreement in the case of mass concentration and n_{250} which provides a confident input in the INP parameterizations by DeMott et al. (2010, 2015). Differences were observed regarding CCN concentrations. The reasons for the differences cannot easily be fixed because many error sources can potentially contribute to the uncertainties. The assumptions in the lidar retrieval lead to an uncertainty range within a factor of

two. The dominating contribution of smoke particles to the CCN concentration in the wintertime SAL could be shown in one example.

As an outlook, more comparisons (lidar versus airborne observations) in different environments are needed to check the quality of the applied CCN and INP parameterizations in the lidar data analysis and also of the airborne in situ observations. Marinou et al. (2018) presented comparisons with unmanned aerial vehicles (UAV) and we will continue our comparisons of lidar and airborne in situ observations that have been simultaneously conducted during the A-LIFE (Absorbing aerosol layers in a changing climate: aging, lifetime and dynamics) campaign in Cyprus in April 2017.

Author contribution

MH analyzed the lidar data, and performed together with DA and AA the lidar measurements. AW, together with MD, DS and BW performed the in situ measurements and analyzed the data. MH prepared the manuscript in close cooperation with AA and helpful comments and discussions of AW and BW. DF enabled the lidar measurements at the CIMH, Barbados.

Acknowledgements. This activity is supported by ACTRIS Research Infrastructure (EU H2020-R&I) under grant agreement number 654109 and by the European Research Council under the European Community's Horizon 2020 research and innovation framework program/ERC grant agreement number 640458 (A-LIFE). The logistical support of the Caribbean Institute for Meteorology and Hydrology (CIMH), Husbands, Barbados, should be acknowledged.

References

Ansmann, A., Wandinger, U., Riebesell, M., Weitkamp, C., and Michaelis, W.: Independent measurement of extinction and backscatter profiles in cirrus clouds by using a combined Raman elastic-backscatter lidar, Appl. Opt., 31, 7113–7131, doi:10.1364/AO.31.007113, 1992.

Ansmann, A., Baars, H., Tesche, M., Müller, D., Althausen, D., Engelmann, R., Pauliquevis, T., and Artaxo, P.: Dust and smoke transport from Africa to South America: Lidar profiling over Cape Verde and the Amazon rainforest, Geophysical Research Letters, 36, L11 802, doi:10.1029/2009GL037923, http://dx.doi.org/10.1029/2009GL037923, 2009.

Ansmann, A., Rittmeister, F., Engelmann, R., Basart, S., Jorba, O., Spyrou, C., Remy, S., Skupin, A., Baars, H., Seifert, P., Senf, F., and Kanitz, T.: Profiling of Saharan dust from the Caribbean to western Africa – Part 2: Shipborne lidar measurements versus forecasts, Atmospheric Chemistry and Physics, 17, 14 987–15 006, doi:10.5194/acp-17-14987-2017, https://www.atmos-chem-phys.net/17/14987/2017/, 2017.

Ansmann, A., Mamouri, R.-E., Hofer, J., Baars, H., Althausen, D., and Abdullaev, S. F.: Dust mass, CCN, and INP profiling with polarization lidar: Updated POLIPHON conversion factors from global AERONET analysis, Atmospheric Measurement Techniques Discussions, 2019, 1–28, doi:10.5194/amt-2019-98, https://www.atmos-meas-tech-discuss.net/amt-2019-98/, 2019.

Baars, H., Ansmann, A., Althausen, D., Engelmann, R., Artaxo, P., Pauliquevis, T., and Souza, R.: Further evidence for significant smoke transport from Africa to Amazonia, Geophysical Research Letters, 38, L20 802, doi:10.1029/2011GL049200, http://dx.doi.org/10.1029/2011GL049200, 2011.

Baumgardner, D., Jonsson, H., Dawson, W., O'Connor, D., and Newton, R.: The cloud, aerosol and precipitation spectrometer: a new instrument for cloud investigations, Atmospheric Research, 59-60, 251 – 264, doi:https://doi.org/10.1016/S0169-8095(01)00119-3, http://www.sciencedirect.com/science/article/pii/S0169809501001193, 13th International Conference on Clouds and Precipitation, 2001.

Brock, C. A., Cozic, J., Bahreini, R., Froyd, K. D., Middlebrook, A. M., McComiskey, A., Brioude, J., Cooper, O. R., Stohl, A., Aikin, K. C., de Gouw, J. A., Fahey, D. W., Ferrare, R. A., Gao, R.-S., Gore, W., Holloway, J. S., Hübler, G., Jefferson, A., Lack, D. A., Lance, S., Moore, R. H., Murphy, D. M., Nenes, A., Novelli, P. C., Nowak, J. B., Ogren, J. A., Peischl, J., Pierce, R. B., Pilewskie, P., Quinn, P. K., Ryerson, T. B., Schmidt, K. S., Schwarz, J. P., Sodemann, H., Spackman, J. R., Stark, H., Thomson, D. S., Thornberry, T., Veres, P., Watts, L. A., Warneke, C., and Wollny, A. G.: Characteristics, sources, and transport of aerosols measured in spring 2008 during the aerosol, radiation, and cloud processes affecting Arctic Climate (ARCPAC) Project, Atmospheric Chemistry and Physics, 11, 2423–2453, doi:10.5194/acp-11-2423-2011, https://www.atmos-chem-phys.net/11/2423/2011/, 2011.

Cai, Y., Montague, D. C., Mooiweer-Bryan, W., and Deshler, T.: Performance characteristics of the ultra high sensitivity aerosol spectrometer for particles between 55 and 800nm: Laboratory and field studies, Journal of Aerosol Science, 39, 759 – 769, doi:https://doi.org/10.1016/j.jaerosci.2008.04.007, http://www.sciencedirect.com/science/article/pii/S0021850208000815, 2008.

DeMott, P. J., Prenni, A. J., Liu, X., Kreidenweis, S. M., Petters, M. D., Twohy, C. H., Richardson, M. S., Eidhammer, T., and Rogers, D. C.: Predicting global atmospheric ice nuclei distributions and their impacts on climate, Proceedings of the National Academy of Sciences, 107, 11 217–11 222, doi:10.1073/pnas.0910818107, 2010.

DeMott, P. J., Prenni, A. J., McMeeking, G. R., Sullivan, R. C., Petters, M. D., Tobo, Y., Niemand, M., Möhler, O., Snider, J. R., Wang, Z., and Kreidenweis, S. M.: Integrating laboratory and field data to quantify the immersion freezing ice nucleation activity of mineral dust particles, Atmospheric Chemistry and Physics, 15, 393–409, doi:10.5194/acp-15-393-2015, http://www.atmos-chem-phys.net/15/393/2015/, 2015.

DeMott, P. J., Hill, T. C. J., McCluskey, C. S., Prather, K. A., Collins, D. B., Sullivan, R. C., Ruppel, M. J., Mason, R. H., Irish, V. E., Lee, T., Hwang, C. Y., Rhee, T. S., Snider, J. R., McMeeking, G. R., Dhaniyala, S., Lewis, E. R., Wentzell, J. J. B., Abbatt, J., Lee, C., Sultana, C. M., Ault, A. P., Axson, J. L., Diaz Martinez, M., Venero, I., Santos-Figueroa, G., Stokes, M. D., Deane, G. B., Mayol-Bracero, O. L., Grassian, V. H., Bertram, T. H., Bertram, A. K., Moffett, B. F., and Franc, G. D.: Sea spray aerosol as a unique source of ice nucleating particles, Proceedings of the National Academy of Sciences, 113, 5797–5803, doi:10.1073/pnas.1514034112, 2016.

Denjean, C., Caquineau, S., Desboeufs, K., Laurent, B., Maille, M., Quiñones Rosado, M., Vallejo, P., Mayol-Bracero, O. L., and Formenti, P.: Long-range transport across the Atlantic in summertime does not enhance the hygroscopicity of African mineral dust, Geophysical Research Letters, 42, 7835–7843, doi:10.1002/2015GL065693, 2015.

Düsing, S., Wehner, B., Seifert, P., Ansmann, A., Baars, H., Ditas, F., Henning, S., Ma, N., Poulain, L., Siebert, H., Wiedensohler, A., and Macke, A.: Helicopter-borne observations of the continental background aerosol in combination with remote sensing and ground-based measurements, Atmospheric Chemistry and Physics, 18, 1263–1290, doi:10.5194/acp-18-1263-2018, https://www.atmos-chem-phys.net/18/1263/2018/, 2018.

Freudenthaler, V., Esselborn, M., Wiegner, M., Heese, B., Tesche, M., Ansmann, A., Müller, D., Althausen, D., Wirth, M., Fix, A., Ehret, G., Knippertz, P., Toledano, C., Gasteiger, J., Garhammer, M., and Seefeldner, M.: Depolarization ratio profiling at several wavelengths in pure Saharan dust during SAMUM 2006, Tellus B, 61, 165–179, doi:10.1111/j.1600-0889.2008.00396.x, 2009.

Gasteiger, J., Groß, S., Sauer, D., Haarig, M., Ansmann, A., and Weinzierl, B.: Particle settling and vertical mixing in the Saharan Air Layer as seen from an integrated model, lidar, and in situ perspective, Atmospheric Chemistry and Physics, 17, 297–311, doi:10.5194/acp-17-297-2017, 2017.

Groß, S., Freudenthaler, V., Schepanski, K., Toledano, C., Schäfler, A., Ansmann, A., and Weinzierl, B.: Optical properties of long-range transported Saharan dust over Barbados as measured by dual-wavelength depolarization Raman lidar measurements, Atmospheric Chemistry and Physics, 15, 11 067–11 080, doi:10.5194/acp-15-11067-2015, https://www.atmos-chem-phys.net/15/11067/2015/, 2015.

Haarig, M., Engelmann, R., Ansmann, A., Veselovskii, I., Whiteman, D. N., and Althausen, D.: 1064 nm rotational Raman lidar for particle extinction and lidar-ratio profiling: cirrus case study, Atmospheric Measurement Techniques, 9, 4269–4278, doi:10.5194/amt-9-4269-2016, https://www.atmos-meas-tech.net/9/4269/2016/, 2016.

Haarig, M., Ansmann, A., Althausen, D., Klepel, A., Groß, S., Freudenthaler, V., Toledano, C., Mamouri, R.-E., Farrell, D. A., Prescod, D. A., Marinou, E., Burton, S. P., Gasteiger, J., Engelmann, R., and Baars, H.: Triple-wavelength depolarization-ratio profiling of Saharan dust over Barbados during SALTRACE in 2013 and 2014, Atmospheric Chemistry and Physics, 17, 10 767–10 794, doi:10.5194/acp-17-10767-2017, https://www.atmos-chem-phys.net/17/10767/2017/, 2017a.

Haarig, M., Ansmann, A., Gasteiger, J., Kandler, K., Althausen, D., Baars, H., Radenz, M., and Farrell, D. A.: Dry versus wet marine particle optical properties: RH dependence of depolarization ratio, backscatter, and extinction from multiwavelength lidar measurements during SALTRACE, Atmospheric Chemistry and Physics, 17, 14 199–14 217, doi:10.5194/acp-17-14199-2017, https://www.atmos-chem-phys.net/17/14199/2017/, 2017b.

Herich, H., Tritscher, T., Wiacek, A., Gysel, M., Weingartner, E., Lohmann, U., Baltensperger, U., and Cziczo, D. J.: Water uptake of clay and desert dust aerosol particles at sub- and supersaturated water vapor conditions, Phys. Chem. Chem. Phys., 11, 7804–7809, doi:10.1039/B901585J, http://dx.doi.org/10.1039/B901585J, 2009.

Holben, B., Eck, T., Slutsker, I., Tanré, D., Buis, J., Setzer, A., Vermote, E., Reagan, J., Kaufman, Y., Nakajima, T., Lavenu, F., Jankowiak, I., and Smirnov, A.: AERONET—A Federated Instrument Network and Data Archive for

Aerosol Characterization, Remote Sensing of Environment, 66, 1 – 16, doi:http://dx.doi.org/10.1016/S0034-4257(98)00031-5, http://www.sciencedirect.com/science/article/pii/S0034425798000315, 1998.

IPCC: Climate Change 2013: The Physical Science Basis. Contribution of Working Group 1 to the Fifth Assessment Report of the Intergovernmental Panel on Climate Change, Cambridge University Press, New York, USA, http://www.ipcc.ch/report/ar5/, last access: 14th December, 2017, 2013.

Jung, E., Albrecht, B. A., Feingold, G., Jonsson, H. H., Chuang, P., and Donaher, S. L.: Aerosols, clouds, and precipitation in the North Atlantic trades observed during the Barbados aerosol cloud experiment – Part 1: Distributions and variability, Atmospheric Chemistry and Physics, 16, 8643–8666, doi:10.5194/acp-16-8643-2016, https://www.atmos-chem-phys.net/16/8643/2016/, 2016.

Kandler, K., Schneiders, K., Ebert, M., Hartmann, M., Weinbruch, S., Prass, M., and Pöhlker, C.: Composition and mixing state of atmospheric aerosols determined by electron microscopy: method development and application to aged Saharan dust deposition in the Caribbean boundary layer, Atmospheric Chemistry and Physics, 18, 13 429–13 455, doi:10.5194/acp-18-13429-2018, https://www.atmos-chem-phys.net/18/13429/2018/, 2018.

Koehler, K. A., Kreidenweis, S. M., DeMott, P. J., Petters, M. D., Prenni, A. J., and Carrico, C. M.: Hygroscopicity and cloud droplet activation of mineral dust aerosol, Geophysical Research Letters, 36, doi:10.1029/2009GL037348, https://agupubs.onlinelibrary.wiley.com/doi/abs/10.1029/2009GL037348, 2009.

Kristensen, T. B., Wex, H., Nekat, B., Nojgaard, J. K., van Pinxteren, D., Lowenthal, D. H., Mazzoleni, L. R., Dieckmann, K., Bender Koch, C., Mentel, T. F., Herrmann, H., Gannet Hallar, A., Stratmann, F., and Bilde, M.: Hygroscopic growth and CCN activity of HULIS from different environments, J. Geophys. Res., 117, doi:10.1029/2012jd018249, https://doi.org/10.1029/2012JD018249, 2012.

Kristensen, T. B., Müller, T., Kandler, K., Benker, N., Hartmann, M., Prospero, J. M., Wiedensohler, A., and Stratmann, F.: Properties of cloud condensation nuclei (CCN) in the trade wind marine boundary layer of the western North Atlantic, Atmospheric Chemistry and Physics, 16, 2675–2688, doi:10.5194/acp-16-2675-2016, http://www.atmos-chem-phys.net/16/2675/2016/, 2016.

Kumar, P., Sokolik, I. N., and Nenes, A.: Measurements of cloud condensation nuclei activity and droplet activation kinetics of fresh unprocessed regional dust samples and minerals, Atmospheric Chemistry and Physics, 11, 3527–3541, doi:10.5194/acp-11-3527-2011, https://www.atmos-chem-phys.net/11/3527/2011/, 2011a.

Kumar, P., Sokolik, I. N., and Nenes, A.: Cloud condensation nuclei activity and droplet activation kinetics of wet processed regional dust samples and minerals, Atmospheric Chemistry and Physics, 11, 8661–8676, doi:10.5194/acp-11-8661-2011, https://www.atmos-chem-phys.net/11/8661/2011/, 2011b.

Kupc, A., Williamson, C., Wagner, N. L., Richardson, M., and Brock, C. A.: Modification, calibration, and performance of the Ultra-High Sensitivity Aerosol Spectrometer for particle size distribution and volatility measurements during the Atmospheric Tomography Mission (ATom) airborne campaign, Atmospheric Measurement Techniques, 11, 369–383, doi:10.5194/amt-11-369-2018, https://www.atmos-meas-tech.net/11/369/2018/, 2018.

Lance, S., Nenes, A., Medina, J., and Smith, J. N.: Mapping the Operation of the DMT Continuous Flow CCN Counter, Aerosol Science and Technology, 40, 242–254, doi:10.1080/02786820500543290, https://doi.org/10.1080/02786820500543290, 2006.

Lieke, K., Kandler, K., Scheuvens, D., Emmel, C., Von Glahn, C., Petzold, A., Weinzierl, B., Veira, A., Ebert, M., Weinbruch, S., and Schütz, L.: Particle chemical properties in the vertical column based on aircraft observations in the vicinity of Cape Verde Islands, Tellus B, 63, 497–511, doi:10.1111/j.1600-0889.2011.00553.x, 2011.

Lv, M., Wang, Z., Li, Z., Luo, T., Ferrare, R., Liu, D., Wu, D., Mao, J., Wan, B., Zhang, F., and Wang, Y.: Retrieval of Cloud Condensation Nuclei Number Concentration Profiles From Lidar Extinction and Backscatter Data, Journal of Geophysical Research: Atmospheres, 123, 6082–6098, doi:10.1029/2017JD028102, https://agupubs.onlinelibrary.wiley.com/doi/abs/10.1029/2017JD028102, 2018.

Mamouri, R. E. and Ansmann, A.: Fine and coarse dust separation with polarization lidar, Atmospheric Measurement Techniques, 7, 3717–3735, doi:10.5194/amt-7-3717-2014, https://www.atmos-meas-tech.net/7/3717/2014/, 2014.

Mamouri, R.-E. and Ansmann, A.: Potential of polarization lidar to provide profiles of CCN- and INP-relevant aerosol parameters, Atmospheric Chemistry and Physics, 16, 5905–5931, doi:10.5194/acp-16-5905-2016, https://www.atmos-chem-phys.net/16/5905/2016/, 2016.

Mamouri, R.-E. and Ansmann, A.: Potential of polarization/Raman lidar to separate fine dust, coarse dust, maritime, and anthropogenic aerosol profiles, Atmospheric Measurement Techniques, 10, 3403–3427, doi:10.5194/amt-10-3403-2017, https://www.atmos-meas-tech.net/10/3403/2017/, 2017.

Marinou, E., Tesche, M., Nenes, A., Ansmann, A., Schrod, J., Mamali, D., Tsekeri, A., Pikridas, M., Baars, H., Engelmann, R., Voudouri, K.-A., Solomos, S., Sciare, J., Gro, S., and Amiridis, V.: Retrieval of ice nucleating particle concentrations from lidar observations: Comparison with airborne in-situ measurements from UAVs, Atmospheric Chemistry and Physics Discussions, 2018, 1–37, doi:10.5194/acp-2018-1203, https://www.atmos-chem-phys-discuss.net/acp-2018-1203/, 2018.

McCluskey, C. S., Ovadnevaite, J., Rinaldi, M., Atkinson, J., Belosi, F., Ceburnis, D., Marullo, S., Hill, T. C. J., Lohmann, U., Kanji, Z. A., O'Dowd, C., Kreidenweis, S. M., and DeMott, P. J.: Marine and Terrestrial Organic Ice-Nucleating Particles in Pristine Marine to Continentally Influenced Northeast Atlantic Air Masses, J. Geophys. Res. Atmos., 123, 6196–6212, doi:10.1029/2017JD028033, https://doi.org/10.1029/2017JD028033, 2018.

Niemand, M., Möhler, O., Vogel, B., Vogel, H., Hoose, C., Connolly, P., Klein, H., Bingemer, H., DeMott, P., Skrotzki, J., and Leisner, T.: A Particle-Surface-Area-Based Parameterization of Immersion Freezing on Desert Dust Particles, Journal of the Atmospheric Sciences, 69, 3077–3092, doi:10.1175/JAS-D-11-0249.1, http://dx.doi.org/10.1175/JAS-D-11-0249.1, 2012.

Petters, M. D. and Kreidenweis, S. M.: A single parameter representation of hygroscopic growth and cloud condensation nucleus activity, Atmospheric Chemistry and Physics, 7, 1961–1971, doi:10.5194/acp-7-1961-2007, https://www.atmos-chem-phys.net/7/1961/2007/, 2007.

Petters, M. D., Carrico, C. M., Kreidenweis, S. M., Prenni, A. J., DeMott, P. J., Collett Jr., J. L., and Moosmüller, H.: Cloud condensation nucleation activity of biomass burning aerosol, J. Geophys. Res., 114, doi:10.1029/2009jd012353, https://doi.org/10.1029/2009JD012353, 2009.

Roberts, G. C. and Nenes, A.: A Continuous-Flow Streamwise Thermal-Gradient CCN Chamber for Atmospheric Measurements, Aerosol Science and Technology, 39, 206–221, doi:10.1080/027868290913988, https://doi.org/10.1080/027868290913988, 2005.

Schrod, J., Weber, D., Drücke, J., Keleshis, C., Pikridas, M., Ebert, M., Cvetković, B., Nickovic, S., Marinou, E., Baars, H., Ansmann, A., Vrekoussis, M., Mihalopoulos, N., Sciare, J., Curtius, J., and Bingemer, H. G.: Ice nucleating particles over the Eastern Mediterranean measured by unmanned aircraft systems, Atmospheric Chemistry and Physics, 17, 4817–4835, doi:10.5194/acp-17-4817-2017, https://www.atmos-chem-phys.net/17/4817/2017/, 2017.

Shinozuka, Y., Clarke, A. D., Nenes, A., Jefferson, A., Wood, R., McNaughton, C. S., Ström, J., Tunved, P., Redemann, J., Thornhill, K. L., Moore, R. H., Lathem, T. L., Lin, J. J., and Yoon, Y. J.: The relationship between cloud condensation nuclei (CCN) concentration and light extinction of dried particles: indications of underlying aerosol processes and implications for satellite-based CCN estimates, Atmospheric Chemistry and Physics, 15, 7585–7604, doi:10.5194/acp-15-7585-2015, https://www.atmos-chem-phys.net/15/7585/2015/, 2015.

Siebert, H., Beals, M., Bethke, J., Bierwirth, E., Conrath, T., Dieckmann, K., Ditas, F., Ehrlich, A., Farrell, D., Hartmann, S., Izaguirre, M. A., Katzwinkel, J., Nuijens, L., Roberts, G., Schäfer, M., Shaw, R. A., Schmeissner, T., Serikov, I., Stevens, B., Stratmann, F., Wehner, B., Wendisch, M., Werner, F., and Wex, H.: The fine-scale structure of the trade wind cumuli over Barbados – an introduction to the CARRIBA project, Atmospheric Chemistry and Physics, 13, 10 061–10 077, doi:10.5194/acp-13-10061-2013, https://www.atmos-chem-phys.net/13/10061/2013/, 2013.

Spanu, A., Dollner, M., Gasteiger, J., Bui, T. P., and Weinzierl, B.: Flow-induced errors in airborne in-situ measurements of aerosols and clouds, Atmospheric Measurement Techniques Discussions, 2019, 1–46, doi:10.5194/amt-2019-27, https://www.atmos-meas-tech-discuss.net/amt-2019-27/, 2019.

Steinke, I., Hoose, C., Möhler, O., Connolly, P., and Leisner, T.: A new temperature- and humidity-dependent surface site density approach for deposition ice nucleation, Atmospheric Chemistry and Physics, 15, 3703–3717, doi:10.5194/acp-15-3703-2015, http://www.atmos-chem-phys.net/15/3703/2015/, 2015.

Tesche, M., Ansmann, A., Müller, D., Althausen, D., Engelmann, R., Freudenthaler, V., and Groß, S.: Vertically resolved separation of dust and smoke over Cape Verde using multiwavelength Raman and polarization lidars during Saharan Mineral Dust Experiment 2008, Journal of Geophysical Research: Atmospheres, 114, D13 202, doi:10.1029/2009JD011862, 2009.

Tesche, M., Groß, S., Ansmann, A., Müller, D., Althausen, D., Freudenthaler, V., and Esselborn, M.: Profiling of Saharan dust and biomass-burning smoke with multiwavelength polarization Raman lidar at Cape Verde, Tellus B, 63, 649–676, doi:10.1111/j.1600-0889.2011.00548.x, 2011.

Tobo, Y., Prenni, A. J., DeMott, P. J., Huffman, J. A., McCluskey, C. S., Tian, G., Pöhlker, C., Pöschl, U., and Kreidenweis, S. M.: Biological aerosol particles as a key determinant of ice nuclei populations in a forest ecosystem, J. Geophys. Res. Atmos., 118, 10,100–10,110, doi:10.1002/jgrd.50801, https://doi.org/10.1002/jgrd.50801, 2013.

Ullrich, R., Hoose, C., Möhler, O., Niemand, M., Wagner, R., Höhler, K., Hiranuma, N., Saathoff, H., and Leisner, T.: A New Ice Nucleation Active Site Parameterization for Desert Dust and Soot, Journal of the Atmospheric Sciences, 74, 699–717, doi:10.1175/JAS-D-16-0074.1, https://doi.org/10.1175/JAS-D-16-0074.1, 2017.

Walser, A., Sauer, D., Spanu, A., Gasteiger, J., and Weinzierl, B.: On the parametrization of optical particle counter response including instrument-induced broadening of size spectra and a self-consistent evaluation of calibration measurements, Atmospheric Measurement Techniques, 10, 4341–4361, doi:10.5194/amt-10-4341-2017, https://www.atmos-meas-tech.net/10/4341/2017/, 2017.

Weinzierl, B., Ansmann, A., Prospero, J. M., Althausen, D., Benker, N., Chouza, F., Dollner, M., Farrell, D., Fomba, W. K., Freudenthaler, V., Gasteiger, J., Groß, S., Haarig, M., Heinold, B., Kandler, K., Kristensen, T. B., Mayol-Bracero, O. L., Müller, T., Reitebuch, O., Sauer, D., Schäfler, A., Schepanski, K., Spanu, A., Tegen, I., Toledano, C., and Walser, A.: The Saharan Aerosol Long-range Transport and Aerosol-Cloud-Interaction Experiment (SALTRACE): overview and selected highlights, Bulletin of the American Meteorological Society, 98, 1427–1451, doi:10.1175/BAMS-D-15-00142.1, http://journals.ametsoc.org/doi/abs/10.1175/BAMS-D-15-00142.1, 2017.

Wex, H., Dieckmann, K., Roberts, G. C., Conrath, T., Izaguirre, M. A., Hartmann, S., Herenz, P., Schäfer, M., Ditas, F., Schmeissner, T., Henning, S., Wehner, B., Siebert, H., and Stratmann, F.: Aerosol arriving on the Caribbean island of Barbados: physical properties and origin, Atmospheric Chemistry and Physics, 16, 14 107–14 130, doi:10.5194/acp-16-14107-2016, http://www.atmos-chem-phys.net/16/14107/2016/, 2016.

Zuidema, P., Sedlacek III, A. J., Flynn, C., Springston, S., Delgadillo, R., Zhang, J., Aiken, A. C., Koontz, A., and Muradyan, P.: The Ascension Island Boundary Layer in the Remote Southeast Atlantic is Often Smoky, Geophys. Res. Lett., 45, 4456–4465, doi:10.1002/2017GL076926, https://doi.org/10.1002/2017GL076926, 2018.

Atmos. Chem. Phys. Discuss., https://doi.org/10.5194/acp-2019-466
Manuscript under review for journal Atmos. Chem. Phys.
Discussion started: 21 May 2019

Atmospheric Chemistry and Physics Discussions

Table 1. List of abbreviations, formulas and uncertainties for the lidar-derived input parameter to estimate CCN and INP number concentrations (Mamouri and Ansmann, 2016) and for the separation of fine and coarse mode mass concentration (Mamouri and Ansmann, 2017). For Saharan dust the updated conversion factors of Ansmann et al. (2019) are used. All conversion factors are given for a lidar wavelength of 532 nm. In the following, the indices d, c, and m represent the aerosol types dust (df – fine mode (r<500 nm), dc – coarse mode dust (r>500 nm)), continental and marine particles, respectively. The extinction coefficient is calculated as the product of the lidar ratio S_i (S_d=55 sr, S_c=50 sr, S_m=20 sr) and the backscatter coefficient β_i of the aerosol component i. NC and MC stand for particle number concentration and mass concentration, respectively. The density ρ_d of dust is 2.6 g/cm^3.

Symbol	Name	Formula	Unit	Uncertainty
M_df	fine mode dust MC (r<500 nm)	= $\rho_\mathrm{d}\ c_\mathrm{v,df}(S_\mathrm{d}\beta_\mathrm{df})$ with $c_\mathrm{v,df} = 0.22\ 10^{-12}$Mm	μg m^{-3}	40–60%
M_dc	coarse mode dust MC (r>500 nm)	= $\rho_\mathrm{d}\ c_\mathrm{v,dc}(S_\mathrm{d}\beta_\mathrm{dc})$ with $c_\mathrm{v,dc} = 0.8\ 10^{-12}$Mm	μg m^{-3}	25–35%
$n_\mathrm{50,c}$	NC with r_dry>50 nm (cont.)	= $c_\mathrm{60,c}\ (S_\mathrm{c}\beta_\mathrm{c})^{\chi_\mathrm{d}}$ with $c_\mathrm{60,c} = 12.7$ cm^{-3} *, $\chi_\mathrm{c} = 0.94$	cm^{-3}	Factor of 2
$n_\mathrm{50,m}$	NC with r_dry>50 nm (marine)	= $c_\mathrm{100,\,m}\ (S_\mathrm{m}\beta_\mathrm{m})^{\chi_\mathrm{m}}$ with $c_\mathrm{100,m} = 7.2$ cm^{-3} *, $\chi_\mathrm{m} = 0.85$	cm^{-3}	Factor of 2
$n_\mathrm{100,d}$	NC with r_dry>100 nm (dust)	= $c_\mathrm{100,d}\ (S_\mathrm{d}\beta_\mathrm{d})^{\chi_\mathrm{d}}$ with $c_\mathrm{100,d} = 4.12$ cm^{-3} *, $\chi_\mathrm{d} = 0.83$	cm^{-3}	Factor of 2
n_250	NC with r_dry>250 nm	= $c_{250,i}(S_i\beta_i)$ with $c_\mathrm{250,d} = 0.19$ Mm cm^{-3} $c_\mathrm{290,c} = 0.10$ Mm cm^{-3} $c_\mathrm{500,m} = 0.06$ Mm cm^{-3}	cm^{-3}	30%
s	surface area concentration	= $c_{\mathrm{s},i}(S_i\beta_i)$ with $c_\mathrm{s,d} = 2.4$ Mm μm^2 cm^{-3} $c_\mathrm{s,c} = 2.8$ Mm μm^2 cm^{-3} $c_\mathrm{s,m} = 0.63$ Mm μm^2 cm^{-3}	μm^2 cm^{-3}	30–50%
n_CCN	NC of CCN	= $f_\mathrm{ss,d}n_\mathrm{100,d} + f_\mathrm{ss,\,c}n_\mathrm{50,c} + f_\mathrm{ss,\,m}n_\mathrm{50,m}$ with $f_{0.2\%,i} = 1.0$	cm^{-3}	Factor of 2
n_INP	NC of INP	see literature in Table 2	L^{-1}	Factor of 3

* for an extinction coefficient of 1 Mm^{-1}

Atmos. Chem. Phys. Discuss., https://doi.org/10.5194/acp-2019-466
Manuscript under review for journal Atmos. Chem. Phys.
Discussion started: 21 May 2019

Atmospheric Chemistry and Physics Discussions

Table 2. The INP parameterizations for immersion freezing with their references and valid temperature intervals. In the case of immersion freezing, ice nucleation starts via an INP immersed into a liquid droplet. In this study, only the parameterizations by DeMott et al. (2010, 2015, 2016) are used. The surface area based parameterizations by Ullrich et al. (2017) are just shown for completeness.

	Reference	**Temp. (K)**	**Input**	**Comments**
D10c	DeMott et al. (2010)	238 – 264	$n_{250,c}, T$	continental aerosol
D15d	DeMott et al. (2015)	238 – 252	$n_{250,d}, T$	dust
D16m	DeMott et al. (2016)	243 – 258	$n_{250,m}, T$	marine aerosol
U17d	Ullrich et al. (2017)	243 – 259	s_d, T	dust
U17c	Ullrich et al. (2017)	237 – 255	s_c, T	soot

Table 3. Dry activation diameter d_{act} for various chemical compositions calculated with kappa-Köhler theory (Petters and Kreidenweis, 2007). The κ values are estimated from literature (Ko09 – Koehler et al. (2009), He09 – Herich et al. (2009), Ku11a – Kumar et al. (2011a), Ku11b – Kumar et al. (2011b), Pe&Kr07 – Petters and Kreidenweis (2007), Pe09 – Petters et al. (2009), Kr12 – Kristensen et al. (2012)). The uncertainty in κ reaches up to ± 0.02, especially for processed Saharan dust and organics.

Material	κ	**Reference**	d_{act}(–10°C) nm	d_{act}(0°C) nm	d_{act}(10°C) nm	d_{act}(20°C) nm
Fresh Saharan dust	0.02	Ko09, He09, Ku11a, Ku11b	307	290	275	261
Processed Saharan dust	0.30	Ko09, He09, Ku11a, Ku11b	126	119	113	107
Ammonium sulfate	0.61	Pe&Kr07	100	94	89	85
Ammonium nitrate	0.67	Pe&Kr07	97	91	87	82
Organics lower limit	0.05	Pe&Kr07, Pe09, Kr12	228	216	204	194
Organics upper limit	0.30	Pe&Kr07, Pe09, Kr12	126	119	113	107
Sodium chloride	1.28	Pe&Kr07	78	74	70	66

Atmos. Chem. Phys. Discuss., https://doi.org/10.5194/acp-2019-466
Manuscript under review for journal Atmos. Chem. Phys.
Discussion started: 21 May 2019

Atmospheric Chemistry and Physics Discussions

Table 4. Lidar and Falcon aircraft measurement periods. The mean distance (with standard deviation) of the Falcon from the lidar observation site is given. Local radiosonde launches provide the wind direction (WD) and wind speed (WS) at the altitude of Falcon aircraft.

Date	**Falcon observation**		**Lidar observation**	**Distance**	**WD**	**WS**
	Height asl.(m)	Time (UTC)	Time (UTC)	km	°	m/s
22 June 2013	2238	20:11–20:50	19:28–21:20	91±60	113	9.9
	3369	19:28–20:08	19:28–21:20	94±62	51	1.0
10 July 2013	2594	16:46–16:55	17:01–19:25	130±100*	100	18.0
	3560	18:12–18:21	17:01–19:25	20±7	93	17.9
	4204	17:52–18:10	17:01–19:25	66±45	89	14.5
	4369	16:30–16:40	17:01–19:25	220±2	93	13.8
11 July 2013	2102	14:02–14:13	12:40–14:20	38±7	73	12.8
	2590	13:51–14:01	12:40–14:20	22±13	71	12.8
	4196	13:39–13:47	12:40–14:20	17±11	64	14.7

* consists of two measurement periods, one around 220 km away (16:46–16:55 UTC) and one around 30 km away (18:23–18:32 UTC)

Table 5. Layer mean CCN and INP concentrations (n_{CCN}, n_{INP}) in the upper (>3 km) and lower (2–3 km) part of the SAL from lidar and Falcon (n_{CCN} only). The standard deviation of the layer mean is given. The uncertainty range for the lidar retrieval is a factor of 2 for n_{CCN} and 3 for n_{INP} (not indicated). The immersion freezing INP parameterizations of D15d at a constant temperature are used. CCN concentrations are given for 0.2% water supersaturation (ss). n_{CCN} and n_{INP} values for the observed dust–smoke mixture measured at Barbados on 3 March 2014 are added.

Date	**Height**	n_{CCN} **Falcon**	n_{CCN} **Lidar**	n_{INP} **Lidar**	n_{INP} **Lidar**	n_{INP} **Lidar**
		0.2% ss	0.2% ss	D15d –20°C	D15d –25°C	D15d –30°C
	km	cm^{-3}	cm^{-3}	L^{-1}	L^{-1}	L^{-1}
22 June 2013	2 – 3	158±13	242±74	3±1	26±11	261±107
	3 – 3.6	88±6	144±21	1±1	9±2	87±16
10 July 2013	2 – 3	157±13	291±12	6±1	65±7	664±69
	3 – 4.4	100±5	189±22	3±1	29±4	299±43
11 July 2013	2 – 3	154±11	270±21	5±1	49±4	496±42
	3 – 4.4	107±7	196±18	3±1	30±4	306±40
3 March 2014	2 – 3	–	412±62	1±1	11±4	110±37

Atmos. Chem. Phys. Discuss., https://doi.org/10.5194/acp-2019-466
Manuscript under review for journal Atmos. Chem. Phys.
Discussion started: 21 May 2019

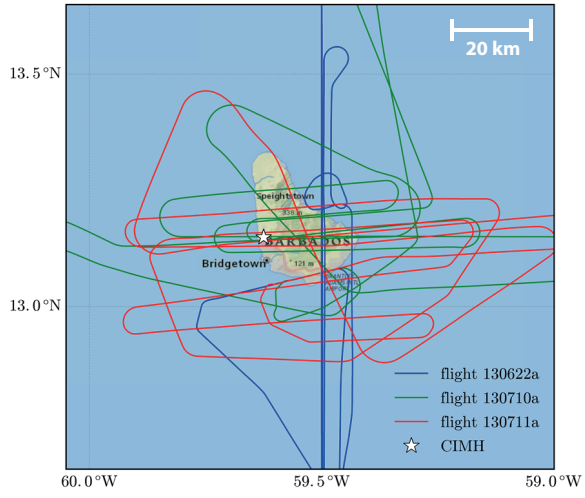

Figure 1. Falcon flight tracks in the Barbados region on 22 June, 10 July, and 11 July 2013. The white star marks the lidar site at the Caribbean Institute for Meteorology and Hydrology (CIMH) north of the capital Bridgetown. Falcon aircraft versus BERTHA lidar comparisons are based on the observations listed in Table 4.

Atmos. Chem. Phys. Discuss., https://doi.org/10.5194/acp-2019-466
Manuscript under review for journal Atmos. Chem. Phys.
Discussion started: 21 May 2019

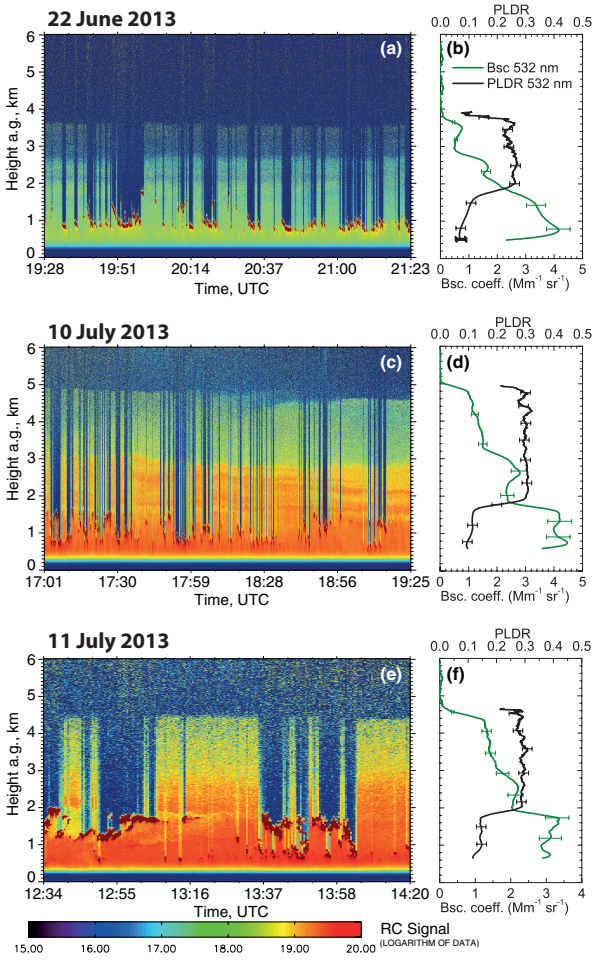

Figure 2. SALTRACE lidar observations of the Saharan air layer (SAL) above the marine boundary layer on 22 June (a-b), 10 July (c-d), and 11 July (e-f) 2013. Time-height displays of the range-corrected signal of the 532 nm cross-polarized channel (left) and the corresponding mean profiles (right) of the particle backscatter coefficient (green line, lower x-axis) and particle linear depolarization ratio (black line, upper x-axis) at 532 nm are shown. Low-level trade wind cumuli (dark red in a, c, e) strongly attenuated the laser light, indicated by the vertically blue column-like areas in a, c, and e. The profiles in b, d, f show cloud-screened mean backscatter coefficients and depolarization ratios. The strong increase of the depolarization ratio indicates the lower boundary of the SAL at approx. 1.8 km height. The top of the SAL was about 3.7 km (22 June), 5.0 km (10 July), and 4.5 km (11 July). Local time is UTC –4 h.

Atmos. Chem. Phys. Discuss., https://doi.org/10.5194/acp-2019-466
Manuscript under review for journal Atmos. Chem. Phys.
Discussion started: 21 May 2019

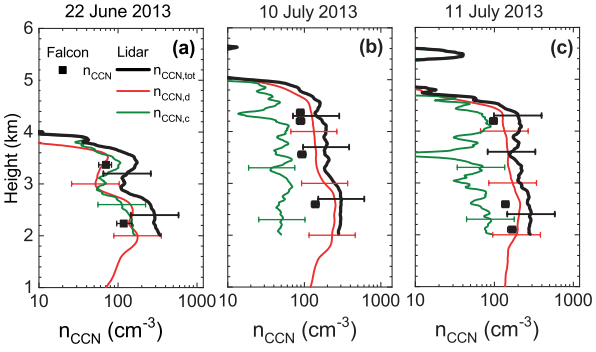

Figure 3. Lidar-derived CCN number concentrations at 0.2% supersaturation (black line) with contributions from dust (red line, critical dry diameter of 200 nm) and continental pollution aerosol (olive line, critical dry diameter of 100 nm) compared to coincident airborne in situ measurements (black dots) during SALTRACE-1. The error bars of the lidar profiles indicate an uncertainty of a factor of 2.

Atmos. Chem. Phys. Discuss., https://doi.org/10.5194/acp-2019-466
Manuscript under review for journal Atmos. Chem. Phys.
Discussion started: 21 May 2019

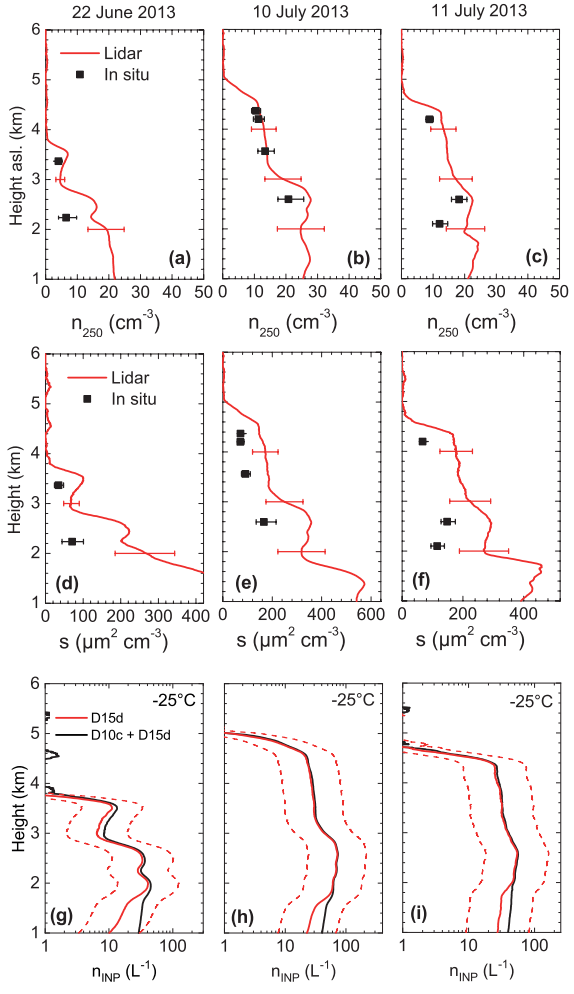

Figure 4. Number concentration n_{250} for particles with radius > 250 nm (a–c) and surface area concentration s (d–f) measured on board the Falcon aircraft (black dots) and derived from the lidar measurements (red profiles, sum of dust and continental pollution particles). The three SALTRACE case studies are shown: 22 June (a,d,g), 10 July (b,e,h), and 11 July 2013 (c,f,i). INP concentrations (g–i) are given at –25°C for the immersion freezing parameterizations of D10c+D15d, and D15d (see Tab. 2). The uncertainty in the lidar-derived n_{250} and s values is 30%. For the INP concentration an uncertainty of a factor 3 is indicated by the dashed lines for the D15d profile.

Atmos. Chem. Phys. Discuss., https://doi.org/10.5194/acp-2019-466
Manuscript under review for journal Atmos. Chem. Phys.
Discussion started: 21 May 2019

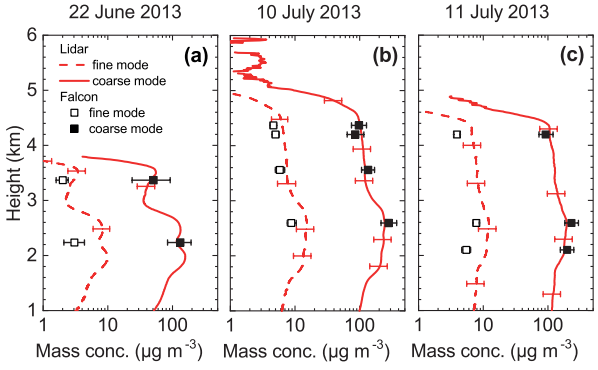

Figure 5. Mass concentration of fine mode (r<500 nm, dashed line) and coarse mode (r>500 nm, solid line) dust derived from airborne in situ measurements (black dots) and lidar observations (red profiles) for the three SALTRACE-1 days.

Atmos. Chem. Phys. Discuss., https://doi.org/10.5194/acp-2019-466
Manuscript under review for journal Atmos. Chem. Phys.
Discussion started: 21 May 2019

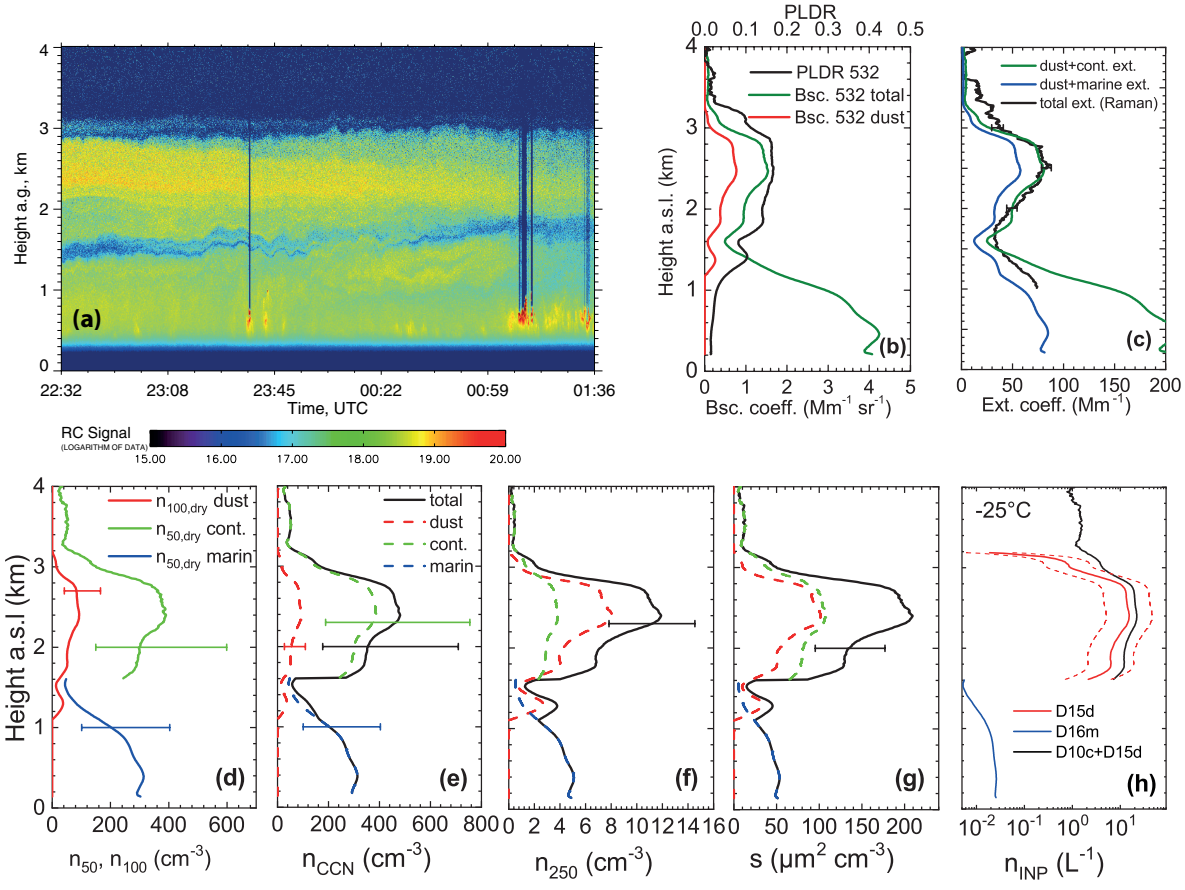

Figure 6. Dust–smoke mixture observed during the SALTRACE winter campaign on 3 March 2014, 22:30–23:20 UTC. (a) Time-height display of the 1064 nm cross-polarized range-corrected signal (only the first 40 min are averaged for the profiles in b–h), (b) particle backscatter coefficient (green line) including its dust contribution (red line) and particle linear depolarization ratio (black line) at 532 nm, (c) sum of dust and continental pollution extinction coefficient (green line) using a smoke lidar ratio of 50 sr and sum of dust and marine particles extinction coefficient (blue line) using a marine lidar ratio of 20 sr compared to the total extinction coefficient (black line) independently measured with BERTHA (Raman lidar method). Above the height of 1.6 km a dust–smoke mixture fits best, below the dust–marine mixture (with a small contribution of smoke or pollution) agrees better with the Raman extinction solution. (d) Number concentration $n_{100,d}$ for dust (red), $n_{50,c}$ for smoke (green), $n_{50,m}$ for marine particles (blue), (e) CCN number concentrations at water supersaturation of 0.2% for the 3 components and the total CCN concentration (black line) above 1.6 km for dust–smoke, below for dust–marine, (f) n_{250} values (colors as before), (g) surface area concentration (colors as before), (h) immersion freezing INP concentrations at –25°C for D10-cont + D15-dust, D15-dust, D16-marine. For the INP concentration an uncertainty of a factor 3 is indicated as dashed lines for the D15d profile.

Atmos. Chem. Phys. Discuss., https://doi.org/10.5194/acp-2019-466
Manuscript under review for journal Atmos. Chem. Phys.
Discussion started: 21 May 2019

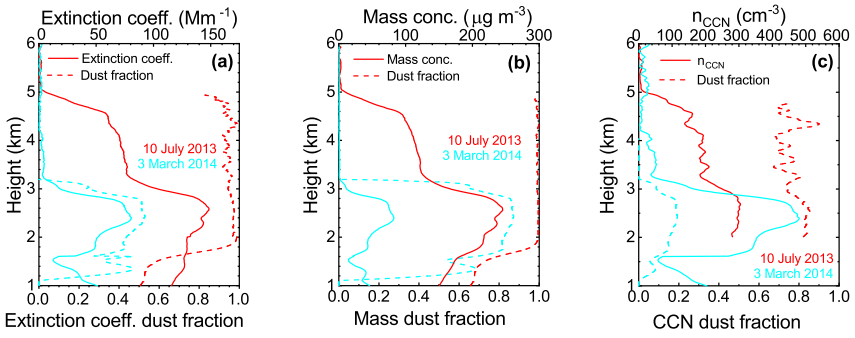

Figure 7. Summer (10 July 2013, red) versus winter (3 March 2014, cyan) aerosol conditions in the SAL. (a) total particle extinction coefficient (solid line) and relative dust contribution to the total particle extinction coefficient (dashed line), (b) same as (a) except for dust mass concentration, (c) same as (a) except for CCN concentration.